**No. 131/24, 7–22**
**ISSN 2657-6988 (online)**
**ISSN 2657-5841 (printed)**
**DOI: 10.26408/131.01**

**Submitted: 02.05.2023**
**Accepted: 13.12.2023**
**Published: 30.09.2024**

# A STOCHASTIC PETRI NET-BASED MODEL OF NON-ENZYMATIC RNA DEGRADATION

**Agnieszka Rybarczyk**
Gdynia Maritime University, Morska 81–87, 81–225 Gdynia, Poland, Faculty of Electrical Engineering, ORCID 0000-0003-4115-0737, e-mail: a.rybarczyk@we.umg.edu.pl

**Abstract:** In recent years, RNA research has grown due to the discovery of its important role in biological systems. RNA molecules are involved in protein synthesis and play a critical role in gene expression. Many of these molecules are produced through the enzymatic digestion or spontaneous degradation of larger molecules, and are consequently essential for cellular processes. The mechanisms of RNA degradation appear to be one of the most important factors influencing RNA activity.
In this study, a stochastic Petri net-based model of spontaneous (non-enzymatic) RNA degradation was built and analysed. The model was analysed using t-invariants, MCT sets, and simulation-based analyses. The systems approach enabled a thorough analysis of the phenomenon, resulting in significant biological insights.

**Keywords:** nonenzymatic RNA hydrolysis, RNA degradation, stochastic Petri net, mathematical modelling, simulation.

## 1. INTRODUCTION

A major breakthrough was made in biology in the latter half of the 20th century, with the discovery of the fundamental processes behind the expression of biological information. The central dogma was created to describe the workings of living organisms, with DNA as the primary genetic information carrier and proteins as the primary building blocks and regulators of gene expression. Initially, RNA was thought to have only a supporting role as an intermediary in protein synthesis and as a scaffold for multi-enzyme complexes [Ross 1995].

Nevertheless, new sequencing techniques have shown that gene expression is more complex than was previously thought. It was found that in animals and plants, protein-coding regions represent only a small portion of the genetic material, and non-coding RNA molecules, such as srRNA (small regulatory RNA), play a significant role in genetic expression [Wang et al. 2017; Zhang et al. 2019]. This has led to ongoing research on RNA functions and a new perspective on the transcriptome [Jackowiak et al. 2011].

Regulatory RNAs, 19–28 nucleotides in length, can be produced through enzymatic cleavage or non-coding RNA degradation [Jackowiak et al. 2011; Rybarczyk et al. 2016]. They regulate RNA transcription and translation, RNA degradation, folding and editing, and genome structure [Zhang et al. 2019].

RNA degradation is a vital process for maintaining cellular homeostasis. It involves the removal of unnecessary RNA, RNA maturation and processing, quality control, and defence against viral infections. There are two types of RNA degradation, namely, non-enzymatic and enzymatic degradation. Research on non-enzymatic RNA degradation began with the discovery of RNA's catalytic properties related to its structure [Bibillo et al. 2000; Kierzek 2001; Simeone et al. 2022]. However, studying such complex issues at the cellular level is not experimentally possible, so researchers initially examined the effect of the spatial structure of RNA on degradation without considering cellular factors. The studies showed that RNA degradation depends on RNA structure and that the degradation pattern of RNA molecules is similar to that resulting from RNA-cutting enzymes (namely ribonucleases). This is likely because proteins that evolved later, favoured and facilitated RNA degradation at the same sites where RNA was initially cleaved [Kierzek 2001; Rybarczyk et al. 2016; 2017].

The RNA degradation mechanisms and protein families are similar in bacteria and higher organisms, and any RNA can be degraded, regardless of its function, indicating that the spatial structure of RNA is critical for its stability in the cell.
Despite numerous described RNA degradation mechanisms, this process remains poorly understood with many unknown aspects [Kumar et al. 2015]. To gain a deeper understanding of this process, novel approaches were employed in the fields of systems biology and medicine, which enabled consideration of various aspects of the investigated phenomenon [Formanowicz et al. 2018; 2020a,b].

Modelling complex biological systems is a challenging process due to the vast number of newly discovered biological facts and the dependencies between them. Additionally, it is necessary to consider that many processes in living organisms' cells occur in parallel, and their elements (substrates, products) may be shared. Mathematical formalisms provide significant help in this regard, enabling the description of the considered system using a particular model and its analysis, which allows for the discovery of previously unknown properties. Additionally, within such a developed model, biologists can change its parameters and then test how this will affect the behaviour of the investigated biological system [Murata 1989; Koch, Reisig and Schreiber 2011].

In this work, Petri nets were used for this purpose, which are intuitive for biologists as they can be represented graphically and are also easy to mathematically analyse. As far as I know, there have not been any studies carried out utilizing stochastic Petri nets to simulate the non-enzymatic RNA degradation process.

## 2. MATERIAL AND METHODS

### 2.1. Petri nets and stochastic Petri nets

This section introduces the basics of Petri nets, which are weighted directed bipartite graphs consisting of places and transitions. Places represent passive components and transitions represent active components, such as chemical compounds and reactions in biological systems. Tokens reside in places and determine the state of the system, whereas the arcs connecting places and transitions represent causal relationships. [Murata 1989; David and Alla 2010; Koch, Reisig and Schreiber 2011].

More formally, a Petri net is 5-tuple $Q = (P, T, F, W, M_0)$, where $P = \{p_1, p_2, \dots, p_n\}$ is a finite set of places, $T = \{t_1, t_2, \dots, t_m\}$ is a set of transitions, $F \subseteq (P \times T) \cup (T \times P)$ is a set of arcs, $W: F \to \mathbb{Z}^+$ is a weight function, $M_0: P \to \mathbb{N}$ is an initial marking, $P \cap T = \emptyset \wedge P \cup T \neq \emptyset$ [Murata 1989].

Tokens move between places and transitions following the firing rule, which requires pre-places to contain enough tokens to match the arc weight. Enabled transitions can then fire, moving tokens from pre-places to post-places with the amount transferred corresponding to the arc weight.

Petri nets have an intuitive graphical representation, where transitions are displayed as rectangles or bars, and places are shown as circles. The connections between places and transitions, or transitions and places, are illustrated as arrows. Tokens, or the entities that move within the system, are depicted as dots or positive integers that are placed in the circles representing places. The weight of the arcs is represented by positive integer numbers. If the weight is equal to one, it is often omitted from the graphical representation of the Petri net [Murata 1989; David and Alla 2010; Koch, Reisig and Schreiber 2011].

Stochastic Petri nets (SPNs) are an extension of the previously mentioned classical Petri nets. Just like classical Petri nets, stochastic nets maintain discrete numbers of tokens in their places. However, in SPNs, a firing rate, which is the waiting time or firing delay, is associated with each transition. This firing time of transition $t_j$ is a random variable $X_j \in [0,\infty)$ that follows an exponential distribution, with $f_{x_j}(\tau) = \lambda_j(m) \cdot e^{-\tau \ (m)\cdot\tau}, \tau \geq 0$ probability density function [Bause and Kritzinger 2013], where $m$ is the number of transitions, and $\tau$ represents the time variable. Thus $f_{x_j}(\tau)$ describes the likelihood of the transition $t_j$ firing at a particular time $\tau$ based on the current marking.

More formally, a stochastic Petri net is 6-tuple $SPN = (P, T, F, W, M_0, v)$, where $(P, T, F, W, M_0)$ is a classical Petri net underlying the SPN. The list of marking dependent firing rates that are associated with transitions is represented by $v = \{\lambda_1, \lambda_2, \dots, \lambda_m\}$, where $m$ is the number of transitions [Marsan 1989]. The firing rates are generally specific to each individual transition and depend on the current state of the system.

A SPN uses mass-action kinetics for transitions, with stochastic rates determined heuristically [Formanowicz 2018]. As exact time dependencies are unknown, four constant times approximating the actual values are used ("very short" – seconds; "short" – seconds to a minute; "medium" – minutes; "long" – longer than half an hour) [Blazewicz et al. 2009]. Next, a time scale ranging from 1 to 100 has been developed based on literature and expert knowledge. Rate constants have been determined by taking the reciprocal of the values on the time scale [Formanowicz, Rybarczyk and Formanowicz 2018].

The stochastic Petri net-based model was evaluated using extensive simulation experiments. The Gillespie stochastic simulation algorithm (SSA), which is implemented in the Snoopy software, was employed for this purpose [Gillespie 1977; Heiner et al. 2012]. The SSA performs a step-by-step simulation of possible steps in the stochastic Petri net, resulting in a valid state of the underlying stochastic process at any time point during the simulation. The number of steps used in the algorithm was determined based on previous analyses. Since each simulation run represents one possible trace of state that changes over time, a significant number of simulation runs are necessary to obtain meaningful results. Thus, the simulation run traces are averaged to accurately represent the system's behavior.

**T-INVARIANTS.** While the graphical depiction of a Petri net is helpful for understanding its structure, it is not the most efficient method for analyzing its mathematical properties. Instead, a different representation called an incidence matrix is utilized. This matrix, denoted as $A = [a_{ij}]_{n \times m}$ consists of $n$ rows (corresponding to places) and $m$ columns (corresponding to transitions). Each entry $a_{ij}$ is an integer that represents the difference between the number of tokens in place $p_i$ after and before the firing transition $t_j$.

In a Petri net model of a biological system, analyzing its invariants is crucial. There are two types of invariants, namely place invariants (p-invariants) and transition invariants (t-invariants). A p-invariant is a solution vector $y \in \mathbb{N}^n$ to the equation $A^T \cdot y = 0$, where $n$ is the number of places. A t-invariant is a solution vector $x \in \mathbb{N}^m$ to the equation $A \cdot x = 0$, where $m$ is the number of transitions.

In this study, I will focus on analyzing t-invariants. Each t-invariant $x$ has a support, denoted by $supp(x)$, which is the set of transitions corresponding to positive entries of $x$. A t-invariant is considered minimal if no other t-invariant's support is a proper subset of its support. A Petri net is considered covered by t-invariants if every transition belongs to the support of at least one t-invariant. The t-invariants correspond to subprocesses that do not change the state of the modeled system and are therefore an important property to study in Petri net analysis.

**MCT SETS.** Transitions in a Petri net can be grouped into maximal common transition sets (MCT sets) based on their t-invariants [Sackmannn, Heiner and Koch 2006]. These MCT sets are disjoint subsets of transitions and divide the net structure into subnets, each corresponding to a functional module of the modeled system. Such a set includes transitions that are part of exactly the same t-invariant supports.

More formally, $\bigvee_{m\in M}\bigvee_{t_i,t_j\in T}(t_i \in m \wedge t_j \in m) \Leftrightarrow \bigvee_{x\in X}\left[(t_i \in supp(x) \wedge t_j \in supp(x)) \vee (t_i \notin supp(x) \wedge t_j \notin supp(x))\right]$, where $X$ is the set of all t-invariants, while $M$ is a collection of all MCT sets [Formanowicz et al. 2022].

Trivial MCT sets containing only one transition are not considered in the analysis. Notably, an MCT set may not necessarily induce a connected subnet, meaning that there may not exist a path containing exactly one place connecting each transition in the set. If an MCT set contains a transition for which such a path does not exist, it induces a non-connected subnet.

The presented analysis excludes trivial MCT sets and mentions an example of a non-connected subnet in the Results and Discussion section.

**KNOCKOUT ANALYSIS.** One important type of Petri net model analysis involves disabling certain parts of the model and studying the behavior of the remaining parts. This approach is known as knockout analysis, which can be classified into two types: t-invariant-based knockout and simulation knockout. In t-invariant-based knockout, selected transitions are disabled, removing certain t-invariants, and the remaining t-invariants are analyzed. This type of analysis enables the identification of the subprocesses affected by the knockout of particular elementary processes (i.e., transitions).

On the other hand, in simulation knockout, selected transitions are knocked out, and the token distribution over a set of places is observed using net simulation. This involves running a series of simulations starting from the same initial token distribution and ending after a specified number of steps. Through knockout analysis, the influence of specific elementary processes (represented by transitions or subsets of transitions) on the behavior of the Petri net can be studied [Grunwald et al. 2008; Formanowicz et al. 2020a,b].

### 2.2. The non-enzymatic RNA degradation phenomena that was taken into account when building the model

RNA molecules are crucial in numerous cellular processes, and their functionality is highly dependent on their hierarchical structure. The primary structure of an RNA is a sequence over the {A,C,G,U} alphabet, where each letter represents a nucleotide (A = adenine, C = cytosine, G = guanine and U = uracil) and the nucleotides are linked by phosphodiester bonds. As RNA folds back onto itself, complementary bases pair up, leading to the formation of its secondary structure. As a result,

RNA can adopt both single-stranded and double-stranded forms, which results in a diverse array of secondary structure elements, such as stems, hairpins, bulges, etc. These elements of the secondary structure are capable of interacting with one another, giving rise to more complex tertiary structures [Rybarczyk et al. 2016, Deng et al. 2023].

Here, a mathematical model based on Petri‘s net theory is presented, proposed and developed by the author of this paper. The model simulates the process of non-enzymatic RNA structure-driven spontaneous degradation according to a description of biochemical experiments [Kierzek 2001; Blazewicz et al. 2011; Rybarczyk et al. 2017].

Their findings indicated that short RNA molecules (oligoribonucleotides) can be specifically and quantitatively cleaved, even in the absence of protein enzymes. They noted that this process is dependent on the structure of the RNA molecule, and the cleavage tends to occur within single-stranded RNA fragments. The presence of labile phosphodiester bonds is crucial for hydrolysis to occur. It was noted that only the phosphodiester bonds between CA, CC, UA, and UC underwent hydrolysis at significant rates. Among these, the bonds between CA and UA were 3 to 5 times more prone to cleavage compared to those between CC and UC. Additionally, the sequences UC, CG, CU, UG, and UU exhibited at least 20 times greater stability than CA, CC, UA, and UC. Under the conditions applied, the phosphodiester bonds AA, AC, AG, AU, GA, GC, GG, and GU remained consistently stable [Kierzek 2001].

Furthermore, studies have demonstrated that the non-enzymatic RNA hydrolysis process is significantly influenced by not only the primary structure but also the secondary and tertiary structure of the substrate [Bibillo et al. 2000; Kierzek 2001].

The exact branch and cut algorithm is described [Rybarczyk et al. 2016], which predicts the stability of RNA molecules based on the RNA sequence and internucleotide bond stability rules proposed by Kierzek et al. [Kierzek 2001] and also operates in a similar manner.

## 3. RESULTS AND DISCUSSION

### 3.1. Model presentation

The proposed model was created using the Holmes tool [Radom et al. 2017], and its structure is shown in Figure 1. The net consists of seven places and 12 transitions, whose numbers and assigned names are described in Tables 1 and 2, respectively.

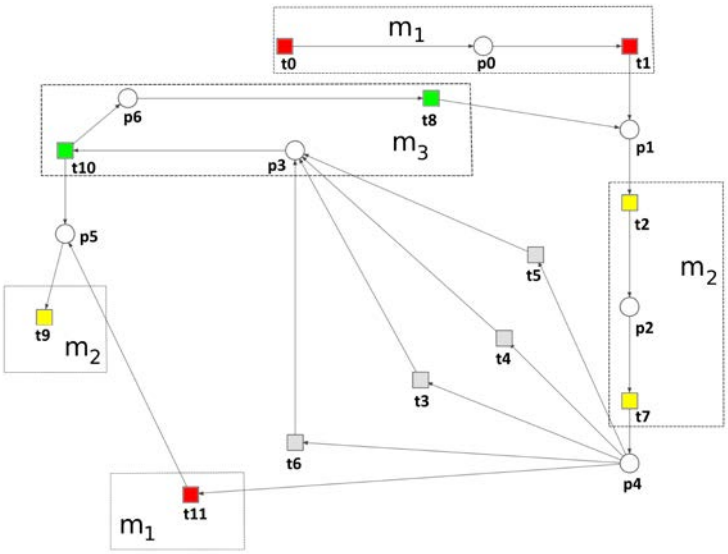


**Fig. 1.** The Petri net-based model of non-enzymatic RNA degradation. The places and transitions are represented by their numbers

*Source: own study.*

**Table 1.** List of places and their biological meaning

| Place | Biological meaning | Place | Biological meaning |
|---|---|---|---|
| $p_0$ | RNA molecule in the solution | $p_4$ | Recognized cleavage sites in single-stranded regions |
| $p_1$ | RNA having a spatial structure | $p_5$ | The resulting degradants |
| $p_2$ | Recognized single-stranded regions | $p_6$ | Fragments longer than 20 nucleotides |
| $p_3$ | RNA fragments resulting from degradation | | |

*Source: own study.*

The model presented above does not take into account quantitative information but only describes the structure of the system under consideration, making it a qualitative (classical) model. Due to the availability of approximate quantitative information on the stability of internucleotide bonds in the RNA molecule, a stochastic Petri net was used as an extension of the discussed model. To do this, the firing rates of each transition had to be estimated.

**Table 2.** List of transitions and their biological meaning

| Transition | Biological meaning | Transition | Biological meaning |
|---|---|---|---|
| $t_0$ | RNA molecule placed in the solution | $t_6$ | Cleavage between nucleotides CG, CU, UG, UU |
| $t_1$ | RNA folding | $t_7$ | Recognition of cleavage sites in single-stranded regions |
| $t_2$ | Identification of single-stranded regions in the RNA structure | $t_8$ | Folding of the resulting single-stranded RNA fragments |
| $t_3$ | Cleavage between nucleotides UA | $t_9$ | Degradants usage |
| $t_4$ | Cleavage between nucleotides CA | $t_{10}$ | Determination of the length of the resulting fragments |
| $t_5$ | Cleavage between nucleotides CC, UC | $t_{11}$ | No allowable cleavage sites are present |

*Source: own study.*

Transitions corresponding to cleavages between individual internucleotide bonds ($t_3$-$t_6$) were assigned kinetic parameters based on defined and calculated degradation measures (degradation membership measures) [Rybarczyk et al. 2016]. Cleavage sites with identical degradation measures were grouped and represented as single transitions in the model. The designated values are as follows: 0.953 for the cleavage site UA ($t_3$), 0.932 for CA ($t_4$), 0.846 for CC, UC ($t_5$), and 0.1 for CG, CU, UG and UU ($t_6$) [Rybarczyk et al. 2016] (c.f. Tab. 4).

**Table 3.** The model's components are assigned approximate durations and time intervals (as indicated in the *Time Information Coming from the Available Literature* and *Time Interval* columns), since precise time values for the modelled processes are unavailable in the literature. To capture the time dependencies between the processes, we used a scale of 1 to 100 (as shown in the *Duration* column)

| Process | Duration | Time Information Coming from the Available Literature | Time Interval |
|---|---|---|---|
| Determination of the length of the resulting fragments | 1 | Seconds [Rybarczyk et al. 2016] | Very short |
| Adoption by an RNA molecule, its spatial structure (folding), recognition of single-stranded regions in the RNA structure, and the locations of cleavage sites | 10 | Seconds to a minute [Rybarczyk et al. 2016] | Short |
| Use of degradants | 80 | Minutes [Watson 2012] | Medium |
| Hydrolysis between nucleotides other than CA, CC, CG, CU, UA, UC, UG or UU | 100 | > Half an hour | Long |

*Source: own study.*

For the remaining transitions, a heuristic [Formanowicz, Rybarczyk and Formanowicz 2018] was used to estimate their kinetic parameters. Due to the lack of precise data regarding the duration of the reactions/processes represented by these transitions, four constant values approximating these durations (on a scale of 1–100) were used and presented in Table 3. The firing rates for transitions were calculated as the inverse of the previously estimated constants (c.f. Tab. 4).

**Table 4.** The rate functions for the analysed model are presented as a list, where MA(c) represents the mass action function [Heiner et al. 2009]. The kinetic parameter (rate constant) is denoted by 'c' and measured in $sec^{-1}$ units. Snoopy [Heiner et al. 2012] provides a predefined function, MA, which generates the rate function for a specific transition using input places and a kinetic parameter as an argument

| Transition | Kinetic Parameter, c | Rate Function | Transition | Kinetic Parameter, c | Rate Function |
|---|---|---|---|---|---|
| $t_0$ | 0.0125 | MA(0.0125) | $t_6$ | 0.1 | MA(0.1) |
| $t_1$ | 0.1 | MA(0.1) | $t_7$ | 0.1 | MA(0.1) |
| $t_2$ | 0.1 | MA(0.1) | $t_8$ | 0.1 | MA(0.1) |
| $t_3$ | 0.953 | MA(0.953) | $t_9$ | 0.0125 | MA(0.0125) |
| $t_4$ | 0.932 | MA(0.932) | $t_{10}$ | 0.1 | MA(0.1) |
| $t_5$ | 0.846 | MA(0.846) | $t_{11}$ | 0.01 | MA(0.01) |

*Source: own study.*

### 3.2. Formal analysis of the model

The structural analysis of the presented model was performed using Holmes software [Radom et al. 2017]. Due to the structural properties of the network, the considered network is pure since it does not have any read arcs (i.e., arcs going in both directions between a place and a transition). Additionally, it is ordinary (and thus homogeneous) since the weight of each arc is equal to 1. The network is also connected, as it is a directed connected graph, but it is not strongly connected. Furthermore, it is not structurally conflict-free, as there are transitions that have common input places, and it is not conservative and bounded, as there is an input transition without predecessors and an output transition without successors.

The net is covered by 5 t-invariants, whose characteristics are included in Table 5, and it does not contain any minimal p-invariants. In the presented model, there are 5 MCT sets, see Table 6.

**Table 5.** The list of t-invariants and their biological meaning. The second column displays all transitions belonging to the support of t-invariants listed in the first column, whereas the third column lists which transitions are contained in the MCT-sets

| t-invariant | Involved transitions | Involved transitions as contained in MCT sets | | |
|---|---|---|---|---|
| | | MCT sets | Single transitions | Biological meaning |
| $x_1$ | $t_2, t_3, t_7, t_8, t_9, t_{10}$ | $m_2$, $m_3$ | $t_3$ | Formation of degradants resulting from the hydrolysis of RNA fragments in single-stranded regions between UA nucleotides |
| $x_2$ | $t_2, t_4, t_7, t_8, t_9, t_{10}$ | $m_2$, $m_3$ | $t_4$ | Formation of degradants resulting from the hydrolysis of RNA fragments in single-stranded regions between CA nucleotides |
| $x_3$ | $t_2, t_5, t_7, t_8, t_9, t_{10}$ | $m_2$, $m_3$ | $t_5$ | Formation of degradants resulting from the hydrolysis of RNA fragments in single-stranded regions between CC, UC nucleotides |
| $x_4$ | $t_2, t_6, t_7, t_8, t_9, t_{10}$ | $m_2$, $m_3$ | $t_6$ | Formation of degradants resulting from the hydrolysis of RNA fragments in single-stranded regions between CG, CU, UG and UU nucleotides |
| $x_5$ | $t_0, t_1, t_2, t_7, t_9, t_{11}$ | $m_1$, $m_2$ | | Formation of degradants resulting from the hydrolysis of RNA fragments in single-stranded regions between nucleotides other than CA, CC, CG, CU, UA, UC, UG, UU |

*Source: own study.*

**Table 6.** The list of MCT sets and their biological meaning

| MCT set | Contained transitions | Biological meaning |
|---|---|---|
| $m_1$ | $t_0$, $t_1$, $t_{11}$ | The process of acquiring spatial structure by the input RNA molecule |
| $m_2$ | $t_2$, $t_7$, $t_9$ | The process of identifying cleavage sites in the single-stranded regions of RNA fragments resulting from the degradation of the input RNA molecule |
| $m_3$ | $t_8$, $t_{10}$ | The process of folding of RNA fragments resulting from the degradation of the input RNA molecule |

*Source: own study.*

In analysing Figure 1, one can notice that the sets $m_1$ and $m_2$ are closely related. The reason why they are not a single MCT set is the presence of a cycle in the analysed model ($p_1 \rightarrow t_2 \rightarrow p_2 \rightarrow t_7 \rightarrow p_4 \rightarrow t_3\ (or\ t_4, t_5, t_6) \rightarrow p_3 \rightarrow t_{10} \rightarrow p_6 \rightarrow t_8 \rightarrow p_1$), which causes transitions from the $m_2$ set, which are part of the cycle, to be activated more frequently than transitions from the $m_1$ set. This is because the token

introduced by the input transition $t_0$ can remain in the cycle, causing the activation of transitions from the $m_3$ and $m_2$ sets each time it passes through it ($t_9$ is always activated because $t_{10}$ produces a token in place $p_6$, reintroducing it into the cycle, and in place $p_5$, where it will be removed from the network by the output transition $t_9$), or it can be directly removed from the network by activating transitions from the $m_1$ and $m_2$ sets ($t_0 \rightarrow p_0 \rightarrow t_1 \rightarrow p_1 \rightarrow t_2 \rightarrow p_2 \rightarrow t_7 \rightarrow p_4 \rightarrow t_{11} \rightarrow p_5 \rightarrow t_9$).

### 3.3. Stochastic simulation and knockout based analysis

To provide a fuller description of the dependencies present in the analysed model, a knockout analysis based on the set of t-invariants was performed using MonaLisa software [Einloft et al. 2013]. Initially, each MCT set (including also trivial ones, such as single transitions) was subjected to a knockout process to evaluate the importance of every functional biological unit in the model. For each MCT set that underwent knockout, the specific transitions that would become inactive were calculated. The outcomes of these calculations, including the number of transitions affected by each knockout, are presented in Table 7.

**Table 7.** Based on the method outlined in [Grunwald et al. 2008; Formanowicz et al. 2020a,b], the activities with the greatest impact on the model as a result of combinatorial knockout were determined

| MCT set | Biological meaning | Knockout Impact (Transitions) [%] | Knockout Impact (t-Invariants) [%] |
|---|---|---|---|
| $m_2$ | The process of identifying cleavage sites in the single-stranded regions of RNA fragments resulting from the degradation of the input RNA molecule | 91.67 | 100 |
| $m_3$ | The process of folding of RNA fragments resulting from the degradation of the input RNA molecule | 41.67 | 80 |
| $m_1$ | The process of acquiring spatial structure by the input RNA molecule | 16.67 | 20 |

*Source: own study.*

Table 7 shows that the exclusion of transitions belonging to the set $m_2$ has a significant impact on the modelled system. Transitions from this set are present in the supports of all computed t-invariants (c.f. Tab. 5). As a result of excluding these transitions, the process of non-enzymatic RNA degradation does not occur.

The degradation of RNA into functional degradation products requires the fragmented RNA to undergo structural degradation. Knocking out transitions from set $m_3$, which belong to 4 out of 5 supports of t-invariants (c.f. Tab. 5), leading to the inhibition of this process (see Fig. 2A).

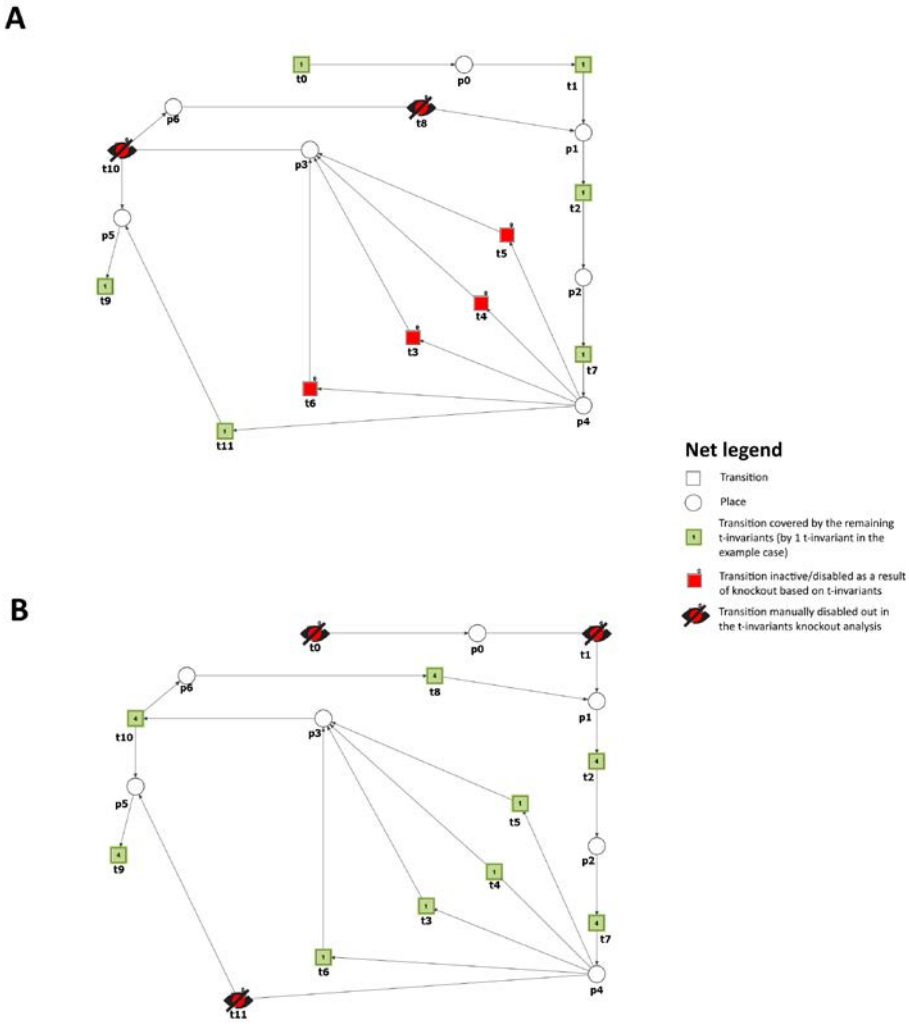


**Fig. 2.** Graphical representation of the t-invariant-based knockout impact: **A.** of the $m_3$, **B.** of the $m_1$. The crossed-out black circles indicate knocked-out transitions, while transitions that belong to the support of any t-invariant are represented as filled green rectangles, with a number inside indicating the number of supports of t-invariants to which the transition belongs. The red rectangles represent transitions that do not belong to the support of any t-invariant. The results were generated using the Holmes software [Radom et al. 2017]

*Source: own study.*

Similarly, acquiring spatial structure by the input RNA molecule is crucial for further non-enzymatic RNA degradation and obtaining final degradation products. Blocking transitions from set $m_1$ should hinder this process. However, the analysis of the results presented in Table 7 does not indicate this (4 t-invariants can still be executed, and all transitions not belonging to set $m_1$ remain active). Further analysis using the Holmes tool [Radom et al. 2017] unequivocally indicates that none of the remaining t-invariants can be executed since the only input transition of model $t_0$ (placing RNA molecule in the solution) has been blocked (see Fig. 2B and 3). In this case, non-enzymatic RNA degradation will not occur.

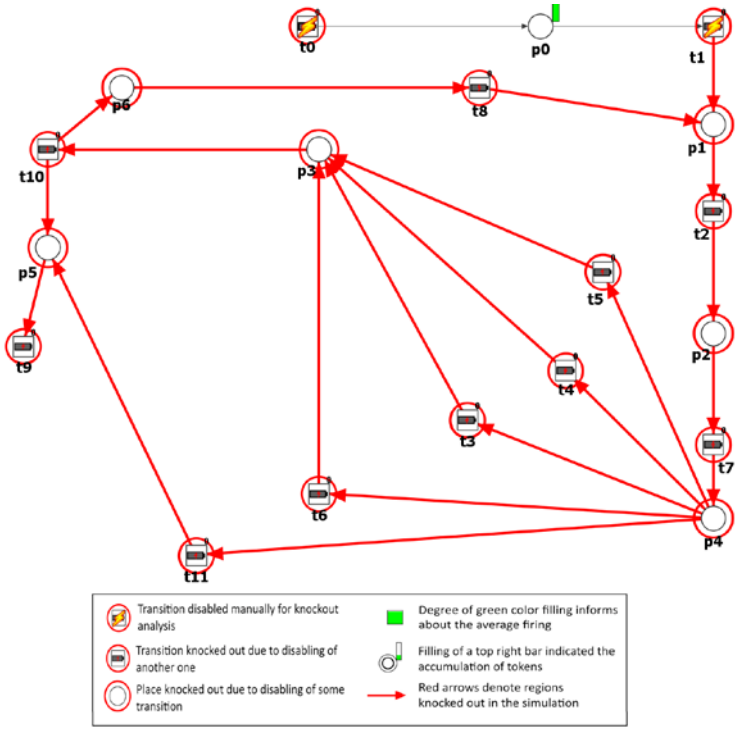


**Fig. 3.** Graphical representation of the knockout results for the entire model, upon disabling of the transitions belonging to $m_1$. Inactive transitions are shown as red circles. The degree of activity change is represented by the level of filling, where partially filled indicates decreased activity, and fully filled indicates unchanged activity compared to the reference set. Holmes software was utilized for the results [Radom et al. 2017]

*Source: own study.*

The next step was to conduct a simulation analysis using the Gillespie stochastic simulation algorithm (SSA) [Gillespie 1977] implemented in the Snoopy software [Heiner et al. 2012]. During the simulation, the number of algorithm steps was set to

100 000, while the results are the average of 50 000 runs [Formanowicz, Rybarczyk and Formanowicz 2018].

In the biochemical experiments presented in Kierzek [2001], it was observed that the internucleotide bonds in RNA molecules exhibit varying susceptibilities to cleavage. The least stable bonds are those between UA, followed by CA. Bonds between CC, UC are hydrolysed more slowly, while bonds between CG, CU, UG and UU are the most stable. These dependencies were described through degradation measures defined and calculated in Rybarczyk et al. [2016]. These values were assigned to transitions corresponding to cleavages between individual internucleotide bonds in the model as their firing rates.

The results of the simulation presented in Figure 4 demonstrate that the relationships regarding the susceptibility to non-enzymatic hydrolysis of the bonds connecting individual nucleotides in the RNA chain have been preserved (UA>CA>(CC, UC)>(CG,UG)>(CU, UU)).

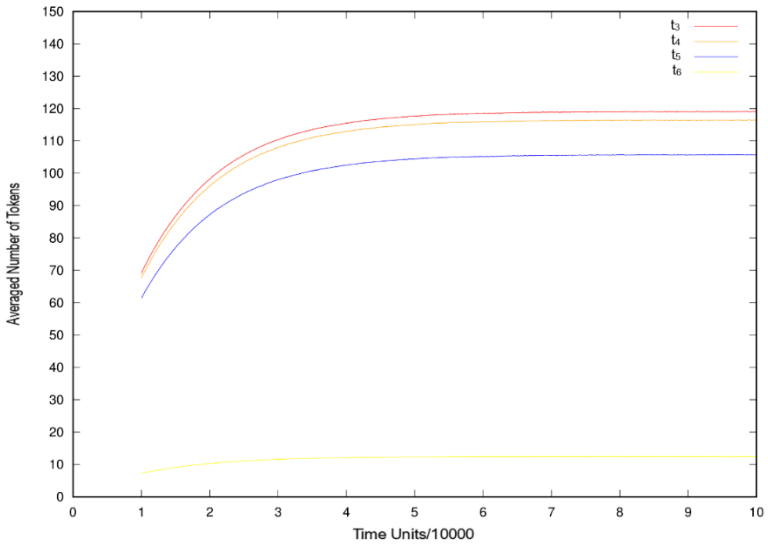


**Fig. 4.** The results of *in silico* knockout analysis for transitions: $t_3$, $t_4$, $t_5$, $t_6$. $t_3$. Simulation for the transition $t_3$. $t_4$. Simulation for the transition $t_4$. $t_5$. Simulation for the transition $t_5$. $t_6$. Simulation for the transition $t_6$

*Source: own study.*

## 4. CONCLUSIONS

In this work, a mathematical model based on the theory of Petri nets was presented, illustrating the course of the process of non-enzymatic RNA degradation, taking into account the spatial structure of RNA, as well as the stability rules proposed by

Kierzek and colleagues (the algorithm presented by Rybarczyk et al. [2016] functions similarly) and based on a biochemical experiment described by Rybarczyk et al. [2016; 2017].

The analysis of the model was based primarily on the knockout analysis based on a set of t-invariants. This allowed for determining the impact of individual processes represented in the model in the course of non-enzymatic RNA degradation.

Next, a simulation analysis of the considered stochastic network was carried out. Transitions corresponding to cleavages between individual nucleotides in the RNA chain were assigned firing rates based on degradation measures defined and calculated in [Rybarczyk et al. 2016]. The results of the stochastic simulation showed that the dependencies related to susceptibility to non-enzymatic hydrolysis of internucleotide bonds in the RNA molecule were preserved (UA>CA>(CC, UC)>(CG, UG)>(CU, UU)).

## REFERENCES


Bause, F., Kritzinger, P., 2013, *Stochastic Petri Nets – An Introduction to the Theory*, Vieveg, Germany.

Bibillo, A., Figlerowicz, M., Ziomek, K., Kierzek, R., 2000, *The Nonenzymatic Hydrolysis of Oligoribonucleotides. VII. Structural Elements Affecting Hydrolysis*, Nucleosides Nucleotides Nucleic Acids, vol. 19, pp. 977–994.

Blazewicz, J., Figlerowicz, M., Kasprzak, M., Nowacka, M., Rybarczyk, A., 2011, *RNA Partial Degradation Problem: Motivation, Complexity, Algorithm*, Journal of Computational Biology, vol. 18, pp. 821–834.

Blazewicz, J., Formanowicz, D., Formanowicz, P., Sackmann, A., Sajkowski, M., 2009, *Modeling the Process of Human Body Iron Homeostasis Using a Variant of Timed Petri Nets*, Discrete Applied Mathematics, vol. 157, no. 10, pp. 2221–2231.

David, R., Alla, H., 2010, *Discrete, Continuous and Hybrid Petri Nets*, Springer, Berlin/Heidelberg, Germany.

Deng, J., Fang, X., Huang, L., Li, S., Xu, L., Ye, K., Zhang, J., Zhang, K., Zhang, Q.C., 2023, *RNA Structure Determination: From 2D to 3D*, Fundamental Research, vol. 3, pp. 727–737.

Einloft, J., Ackermann, J., Nöthen, J., Koch, I., 2013, *MonaLisa – Visualization and Analysis of Functional Modules in Biochemical Networks*, Bioinformatics, vol. 29, pp. 1469–1470.

Formanowicz, D., Radom, M., Rybarczyk, A., Tanaś, K., Formanowicz, P., 2022, *Control of Cholesterol Metabolism Using a Systems Approach*, Biology, vol 11, pp. 430–1–430–33.

Formanowicz, D., Rybarczyk, A., Formanowicz, P., 2018, *Factors Influencing Essential Hypertension and Cardiovascular Disease Modeled and Analyzed Using Stochastic Petri Nets*, Fundamenta Informaticae, vol. 160, pp. 143–165.

Formanowicz, D., Rybarczyk, A., Radom, M., Formanowicz, P., 2020a, *A Role of Inflammation and Immunity in Essential Hypertension-Modeled and Analyzed Using Petri Nets*, International Journal of Molecular Sciences, vol. 21.

Formanowicz, D., Rybarczyk, A., Radom, M., Tanas, K., Formanowicz, P., 2020b, *A Stochastic Petri Net-Based Model of the Involvement of Interleukin 18 in Atherosclerosis*, International Journal of Molecular Sciences, vol. 21, no. 22.

Gillespie, D.T., 1977, *Exact Stochastic Simulation of Coupled Chemical Reactions*, Journal of Physical Chemistry, vol. 81, pp. 2340–2361.

Grunwald, S., Speer, A., Ackermann, J., Koch, I., 2008, *Petri Net Modelling of Gene Regulation of the Duchenne Muscular Dystrophy*, Biosystems, vol. 92, pp. 189–205.

Heiner, M., Herajy, M., Liu, F., Rohr, C., Schwarick, M., 2012, *Snoopy – a Unifying Petri Net Tool*, Lecture Notes in Computer Science, vol. 7347, pp. 398–407.

Heiner, M., Lehrack, S., Gilbert, D., Marwan, W., 2009, *Extended Stochastic Petri Nets for Model-Based Design of Wetlab Experiments*, Transactions on Computational Systems Biology XI; Springer, Berlin/Heidelberg, Germany, vol. 5750, pp. 138–163.

Jackowiak, P., Nowacka, M., Strozycki, P.M., Figlerowicz, M., 2011, *RNA Degradome – Its Biogenesis and Functions*, Nucleic Acids Res, vol. 37, no. 17, pp. 7361–7370.

Kierzek, R., *Nonenzymatic Cleavage of Oligoribonucleotides*, 2001, Methods Enzymology, vol. 341, pp. 657–675.

Koch, I., Reisig, W., Schreiber, F., 2011, *Modeling in Systems Biology. The Petri Net Approach*, Springer, London, UK.

Kumar, P., Mudunuri, S.B., Anaya, J., Dutta, A., 2015, *tRFdb: A Database for Transfer RNA Fragments*, Nucleic Acids Research, vol. 43, pp. D141–D145.

Marsan, M.A., 1989, *Stochastic Petri Nets: An Elementary Introduction*, Lecture Notes in Computer Science, vol. 424, pp. 1–29.

Murata, T., 1989, *Petri Nets: Properties, Analysis and Applications*, Proceedings of the IEEE, vol. 77, pp. 541–580.

Radom, M., Rybarczyk, A., Szawulak, B., Andrzejewski, H., Chabelski, P., Kozak, A., Formanowicz, P., 2017, *Holmes: A Graphical Tool for Development, Simulation and Analysis of Petri Net Based Models of Complex Biological Systems*, Bioinformatics, vol. 33, pp. 3822–3823.

Ross, J., 1995, *mRNA Stability in Mammalian Cells*, Microbiol Rev, vol. 59, pp. 423–450.

Rybarczyk, A., Hertz, A., Kasprzak, M., Blazewicz, J., 2017, *Tabu Search for the RNA Partial Degradation Problem*, International Journal of Applied Mathematics and Computer Science, vol. 27, no. 2, pp. 401–415.

Rybarczyk, A., Jackowiak, P., Figlerowicz, M., Blazewicz, J., 2016, *Computational Prediction of Non-Enzymatic RNA Degradation Patterns*, Acta Biochimica Polonica, vol. 63, no. 4, pp. 745–751.

Sackmann, A., Heiner, M., Koch, I., 2006, *Application of Petri Net Based Analysis Techniques to Signal Transduction Pathway*, BMC Bioinform, vol. 7.

Simeone, I., Rubolino, C., Noviello, T.M.R., Farinello, D., Cerulo, L., Marzi, M.J., Nicassio, F., 2022, *Prediction and Pan-Cancer Analysis of Mammalian Transcripts Involved in Target Directed miRNA Degradation*, Nucleic Acids Res, vol. 50, no. 4, pp. 2019–2035.

Wang, J., Samuels, D.C., Zhao, S., Xiang, Y., Zhao, Y.Y., Guo, Y., 2017, *Current Research on Non-Coding Ribonucleic Acid (RNA)*, Genes, vol. 8, no. 12.

Watson, R.R., 2012, *DHEA in Human Health and Aging*, CRC Press, Boca Raton, USA.

Zhang, P., Wu, W., Chen, Q., Chen, M., 2019, *Non-Coding RNAs and their Integrated Networks*, Journal of Integrative Bioinformatics, vol. 16, no. 3.